Check for updates

**Iván Monge-Concepción**
Department of Mechanical Engineering,
The Pennsylvania State University,
University Park, PA 16802
e-mail: ivan.monge1989@gmail.com

**Michael D. Barringer**[1]
Department of Mechanical Engineering,
The Pennsylvania State University,
University Park, PA 16802
e-mail: mbarringer@psu.edu

**Reid A. Berdanier**
Department of Mechanical Engineering,
The Pennsylvania State University,
University Park, PA 16802
e-mail: rberdanier@psu.edu

**Karen A. Thole**
Department of Mechanical Engineering,
The Pennsylvania State University,
University Park, PA 16802
e-mail: kthole@psu.edu

**Christopher Robak**
Pratt & Whitney,
East Hartford, CT 06118
e-mail: christopher.robak@prattwhitney.com

# Use of Multiple Tracer Gases to Quantify Vane Trailing Edge Flow Into Turbine Rim Seals

*Overlapping features are commonly used as rim seals between stationary and rotating components in a turbine stage. These rim seals are used to prevent main gas path ingestion to the wheelspace cavity, which reduces the lifespan of critical engine components such as the turbine disk. In addition to the overlapping features, purge flow, diverted from the compressor, is injected into the rim cavity to act as an airflow sealing mechanism. Previous research identified that in addition to the purge flow in the rim cavity, cooling flow from the vane trailing edge (VTE) is ingested into the rim seal cavity carrying the potential to cool components in the wheelspace. These previous findings, however, were not able to distinctly separate purge from VTE cooling flows, which is the contribution of this paper based on uniquely using two different tracer gases. A one-stage test turbine operating at engine-relevant conditions and consisting of real engine hardware was used to validate and quantify the ingestion of the VTE flow by independently seeding the purge and VTE flows with two different tracer gases. Experimental results show the presence of VTE flow in the rim seal throughout all purge flowrates evaluated. Circumferential variation of VTE flow was also studied both experimentally and computationally using a computational fluid dynamics model. Results showed that ingested VTE flow can reduce the detrimental effect of hot gas ingestion particularly at higher purge flowrates.* [DOI: 10.1115/1.4055445]

*Keywords: cavity and leaking flows, fluid dynamics and heat transfer phenomena in compressor and turbine components of gas turbine engines, impact on cavity leaking flows on performance*

## Introduction

To achieve carbon neutrality and develop clean forms of energy, gas turbine designers continue to push toward increased turbine thermal efficiencies. Higher efficiencies are achieved, in part, by further increasing the turbine inlet temperatures beyond the melting point of the alloys present in the already mechanically and thermally stressed turbine components. To prevent catastrophic engine failure due to thermal stresses, flow is bled from the upstream compressor and used in the turbine secondary airflow system as cooling flow and as high pressure sealing in the interstage cavities.

To protect, the wheelspace overlapping geometric features called rim seals are used to prevent hot gas ingestion from the main gas path (MGP). Although rim seals have been proven to provide some protection of the hot gases, a portion of the secondary air flow called purge flow is also used to pressurize the cavity aimed at preventing hot gas ingestion. The physics involved in hot gas ingestion, the use of different rim sealing features, and the use of purge flow have been studied extensively to understand the flow physics and provide empirical models for designers [1,2]. Although these models have served as an effective tool to design rim seals, the experimental results show deviation from the models at certain purge flow conditions. Such models also do not take into account other leakage flows, for example, the potential of vane trailing edge (VTE) flow ingress into the rim seal.

The use of VTE flow is commonly used in gas turbines to cool the vane trailing edge metal and to fill the flow deficit left by the vane wake. The effect of VTE flow on rim sealing performance has been studied to a limited degree. Results have shown that VTE flow has the potential of decreasing the fluid temperatures in the rim seal [3]. Time-resolved results have revealed that the presence of VTE flow decreases unsteady pressure amplitudes in the rim seal that originate from Kelvin–Helmholtz cells, which form due to the mismatch in tangential flow velocity between the rim seal flow and main gas path flow. This paper presents a unique study in which rim sealing and rim cooling effectiveness were determined for varying purge and VTE flowrates using a single-stage test turbine that operates at engine-relevant conditions with engine-realistic geometries. To validate the contribution of VTE flow, which was found missing from previous literature reviews [4], two independent tracer gases were used in the current study including carbon dioxide ($CO_2$) for the rim seal purge flow and sulfur hexafluoride ($SF_6$) for the VTE flow. The sulfur hexafluoride was validated as a tracer gas in a benchtop experiment and compared with previous measurements in the test turbine using $CO_2$. Several cooling flow and seeding configurations were defined to determine individual contributions of each flow to concentration effectiveness levels. A computational fluid dynamics (CFD) model of the test turbine was also used to further understand the migration of VTE flow into the rim seal.

## Background Studies

Rim seal geometries are inherently complex to prevent main gas path ingestion and minimize the likelihood of catastrophic component failures in the vulnerable wheelspace cavity. Although there is a great extent of research summarized by Johnson et al. [5] and Scobie et al. [4] aimed at understanding ingestion, relatively few empirical models are available for engine designers to predict ingestion.

The most significant drivers of hot gas ingestion are rotationally induced [1] due to disk pumping effects originating from the wheelspace cavity and externally induced [2] due to the circumferential variation of pressure in the turbine main annulus originating from the airfoils. Empirical models based on these two main ingestion

[1]Corresponding author.

Contributed by the International Gas Turbine Institute (IGTI) of ASME for publication in the Journal of Turbomachinery. Manuscript received July 20, 2022; final manuscript received August 27, 2022; published online October 7, 2022. Tech. Editor: David G. Bogard.

 Copyright © 2022 by ASME 

Downloaded from http://asmedigitalcollection.asme.org/turbomachinery/article-pdf/145/1/011006/6925311/turbo_145_1_011006.pdf by The Pennsylvania State University user on 03 January 2023

drivers and validation experiments using simplified geometries were developed and summarized by Sangan et al. [6,7]. In their empirical model, the rim seal is described as a system of orifices in which ingestion occurs through one orifice and egress occurs through the other orifice. Ingestion equations were derived, and the inertial effects were found to be more significant compared to the viscous forces. The orifice model quantifies rim sealing effectiveness ($\varepsilon$) by relating the ingress/egress ratio of discharge, $\Gamma_c$, to the non-dimensional sealing flowrate required to seal the rim seal cavity, $\Phi/\Phi_{min}$. Furthermore, the experimental studies found that the ingestion mechanisms involved in hot gas ingress are unsteady and three dimensional. Despite this, the data and model shown in these studies confirm and validate the simple orifice model equations for similar turbine stage velocity triangles.

Experimental studies carried out at various turbine facilities have found divergence from such a proposed orifice model as described by Clark et al. [8]. The model was found to under predict the experimental data trends in the regions close to the rim seal entrance. In contrast, at rim seal locations close to the sealing airflow injection, the model was found to over predict the experimental data. Similarly, additional studies from various authors [9–12] have shown an area in which there is an inflection shape in the rim sealing effectiveness curve where an increase in sealing flowrate does not correspond to an increase in rim sealing effectiveness. The discrepancy between the model prediction and the experimental data can be attributed to instabilities present in the rim seal cavity as described by Hualca et al. [13]. Although these instabilities have been studied by several authors, they are currently not well understood.

The general trend of the inflection shape in the rim sealing effectiveness curve was further studied from a time-resolved perspective using fast-response pressure and temperature transducers by Siroka et al. [3] and Monge-Concepción et al. [14]. In their studies, the authors found that pressure amplitudes were the highest at the inflection region for sealing effectiveness and the lowest at sealing flowrates corresponding to a fully purged cavity. These same studies uniquely included the VTE flow to determine its effect on the complex flowfield in the rim seal cavity. Their studies indicated that the presence of VTE flow did not affect the rotational velocity of the large-scale cell structures and cell count in the rim seal cavity but did, however, suppress the unsteady pressure amplitudes. Additionally, a decrease in temperature in the rim seal was identified when VTE flow was present further substantiating the ingestion of the VTE flow into the rim seal region.

An initial study by the authors [15] used specific seeding configurations of the $CO_2$ tracer gas to quantify the contribution of purge and VTE flow on rim cooling effectiveness, $\varepsilon_{cc}$. Note that cooling effectiveness was deduced through concentration measurements of the tracer gas. The results indicated the presence of VTE flow across all radial locations in the wheelspace cavity when VTE flow was held constant at a nominal flowrate. The presence of VTE flow in the rim seal was found to decrease with increasing purge flowrates. Though the previous study was the first in open literature in determining the influence of VTE flow in the rim seal, the use of a single tracer gas limited understanding the independent contributions of each flow in the wheelspace cavity. The goal of the current study is to validate the use of dual tracer gases to determine the influence of each cooling flow present in the rim seal. $SF_6$ was used as the tracer for the VTE flow while $CO_2$ was used as the tracer for the purge flow. For the first time in open literature, a full profile of the purge sealing flow, VTE cooling flow, and hot gas mass fractions is reported in the rim seal at various cooling flowrates. The uniqueness of this study is the use and validation of two distinct tracer gases to quantify the presence of two independent secondary flows in the rim seal region.

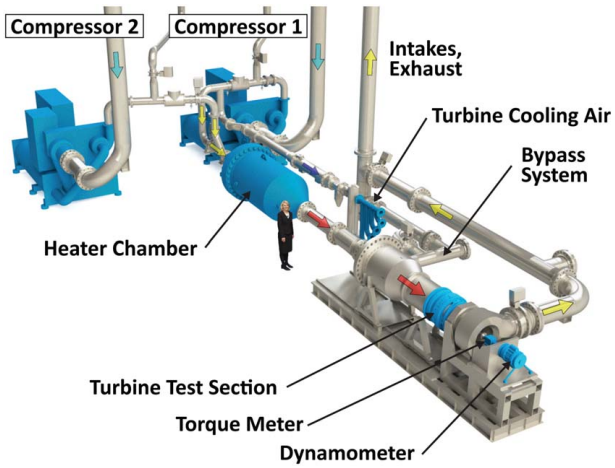


**Fig. 1 Solid model of the START facility showing the main components**

## Experimental Methods

Experiments presented in this paper were performed using the turbine rig at Pennsylvania State University's Steady Thermal Aero Research Turbine (START) Lab. The START facility is an open-loop, continuous, steady-state turbine rig that operates with real engine hardware running at engine-relevant Reynolds and Mach numbers. The facility was designed to study and improve understanding of underplatform sealing, innovate cooling technologies, advance additive manufacturing, and develop novel instrumentation. Details of the design of the turbine facility have been described by Barringer et al. [16].

Figure 1 illustrates the main components of the START facility. Two industrial-sized compressors powered by 1.1 MW (1500 hp) motors supply compressed air to the turbine main gas path and secondary cooling airflow system for a combined airflow rate of up to 11.4 kg/s (25 lbm/s). Each of the compressors can discharge flow at 480 kPa and 395 K (70 psig, 250 °F). A natural gas burner is installed downstream of the compressor discharge before the main gas path flow enters the turbine test section. The burner can increase the air temperature from 395 K to 670 K (250 °F to 750 °F). Data presented in this study did not use the burner to elevate temperatures beyond the compressor discharge temperature. A fraction of the air discharged from one compressor is redirected into the secondary airflow system. A chiller thermally conditions the secondary air to temperatures as low as 273 K (32 °F). Subsequently, the secondary airflow is divided into multiple independently controlled and metered airflow lines, which are delivered to several locations within the test turbine section.

Figure 2 shows a cross-sectional render of the turbine test section depicting the primary and secondary flows present. For this study, two independently controlled secondary flows were present including purge flow (location e) and VTE flow (g). The tangential on-board injection disk flow (h) was not included in this study. Purge flow was delivered axially into the rim seal cavity (c) through 150 equally spaced holes in the circumferential direction. The VTE flow was injected into the main gas path through slots spanning radially from hub to tip in the vane trailing edge. The inner and outer vane plenums (locations (a) and (f), respectively) were sealed and isolated from the MGP flow to prevent ingestion through the vane seals. The vane inner and outer plenums were also isolated and sealed to avoid cross-leak flow from one plenum to the other.

**Turbine Instrumentation.** Included in the START vane assembly were four additively manufactured (AM) doublets, which provided the ability to spatially position pressure taps in the vanes at discrete locations in the main gas path, rim seal, and rim seal cavity. The AM vanes were designed to include internal channels connecting the surface pressure taps in the vane to Teflon tubing external to the test turbine and ultimately to the $CO_2$ and $SF_6$ gas

Downloaded from http://asmedigitalcollection.asme.org/turbomachinery/article-pdf/145/1/011006/6925311/turbo_145_1_011006.pdf by The Pennsylvania State University user on 03 January 2023

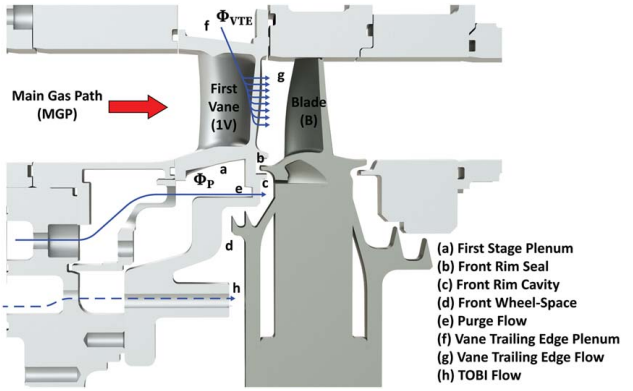


**Fig. 2 Cross-sectional diagram of the single-stage test turbine showing the main gas path and secondary flow paths**

analyzers. The four AM doublets were spaced in the vane ring assembly with two doublets on opposing sides of the assembly.

Figure 3 shows the turbine rig instrumentation and measurement locations used in this study. Single element Kiel probes with a 1.6 mm (0.063 in.) diameter were installed at the turbine inlet to measure pressure and background concentration levels of $CO_2$ and $SF_6$. Static pressure taps were located in the inner and outer vane plenums to measure purge and VTE plenum pressures and the $CO_2$ and $SF_6$ supply concentrations. A series of pressure taps were included in the AM vanes to measure pressure and tracer gas concentrations radially and circumferentially at locations in the rim seal, rim seal cavity, and wheelspace cavity. Temperature probes were also installed in the plenums.

**Tracer Gas Descriptions.** The $CO_2$ and $SF_6$ tracer gases were injected into the secondary airflow system as shown in Fig. 4. The $CO_2$ was injected into the purge flow, and $SF_6$ was injected into the VTE flow as shown by the supply lines. Both purge and VTE flows were seeded independently and supply concentration was measured at various circumferential locations in each of the plenums to ensure concentration uniformity. Tracer gas samples were collected from the independent pressure taps in the rim seal and cavity, and Kiel probes at the turbine inlet. Each flow sample was split to collect simultaneous concentration measurements of both $CO_2$ and $SF_6$ gases. Tracer gas samples were collected at sampling flowrates that followed the methodology by Clark et al. [17] to maintain isokinetic conditions. The use of $SF_6$ as a tracer gas was

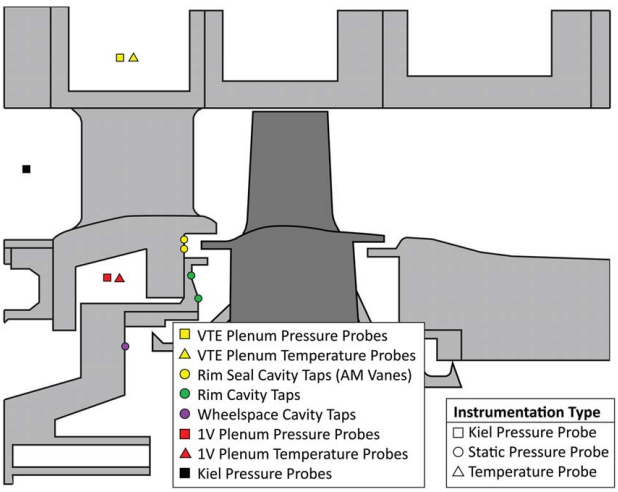


**Fig. 3 Turbine instrumentation layout including pressure, temperature, and Kiel probes**

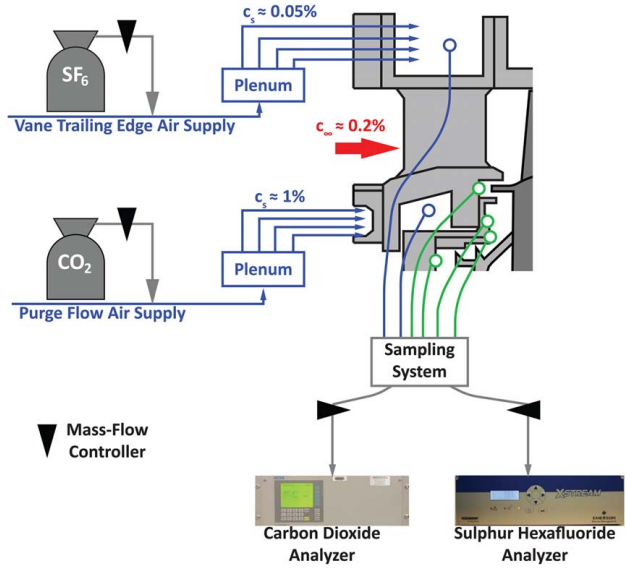


**Fig. 4 Tracer gas ($CO_2$ and $SF_6$) injection and sampling systems**

validated in this study and will be further described in a later section.

The tracer gas $CO_2$ has been used in previous studies by the authors and by others to quantify rim sealing effectiveness ($\varepsilon$), which is based on a mass transfer analogy. The mass flow sealing is characterized by taking volumetric concentration measurements of the flow in terms of individual tracer gas composition. Concentration effectiveness ($\varepsilon_c$) is used as a proxy for mass transfer.

The conventional definition of rim sealing effectiveness includes the purge flow seeding concentration, $c_s$, the main gas path concentration, $c_\infty$, and the local concentration, $c$, at a discrete location. This definition was used to determine rim sealing effectiveness when a single cooling flow, such as the purge flow, was supplied from the vane plenum and injected into the rim seal cavity. A $CO_2$ molar concentration by volume, $c$, was measured from discrete pressure taps in the rim cavity to calculate rim sealing effectiveness. Background concentration of $CO_2$ was measured at the vane inlet, $c_\infty$, using a Kiel probe installed at the turbine entrance, as shown in Fig. 3. The purge flow supply concentration of $CO_2$, $c_s$, was measured within the vane purge plenum using static pressure taps. Effectiveness results shown throughout this study were circumferentially averaged for each radial location.

When VTE flow is present, it will mix with the main gas path flow before arriving at the rim seal entrance, and therefore the conventional definition of rim sealing effectiveness does not apply since $c_\infty$ will be some combination of VTE flow and main gas path flow. For this scenario that includes a mixed background concentration downstream of the VTE (main gas path side of the rim seal), the rim cooling effectiveness $\varepsilon_{cc}$ was used as defined in the nomenclature and Ref. [15]. Furthermore, since two secondary cooling flows were used in this study (purge and VTE flow), the rim cooling effectiveness was calculated for each cooling flow. The contribution of the purge flow to rim cooling effectiveness is designated $\varepsilon_{cc,p}$ and the contribution of the VTE flow to rim cooling effectiveness is designated $\varepsilon_{cc,\mathrm{VTE}}$ as defined in the nomenclature.

As previously mentioned, $SF_6$ was chosen to be the VTE tracer gas for this study which has been used previously in industry applications [18,19]. One of the advantages of using $SF_6$ as a tracer gas is that it is a synthetic gas and therefore the concentrations of $SF_6$ in the atmosphere are minimal, on the order of 10 ppt (parts-per-trillion) [20]. The background concentration of $SF_6$ ($c_{\infty,\mathrm{in}}$) in the main gas path at the vane inlet was measured to be $c_{\infty,\mathrm{in}} \approx 0$ ppm. This provides an advantageous condition in which

Downloaded from http://asmedigitalcollection.asme.org/turbomachinery/article-pdf/145/1/011006/6925311/turbo_145_1_011006.pdf by The Pennsylvania State University user on 03 January 2023

**Table 1 Turbine operating conditions**

| Parameters | Symbol | Value |
|---|---|---|
| Vane inlet Mach number | | 0.1 |
| Vane inlet axial Reynolds number | $Re_x$ | $1.1 \times 10^5$ |
| Blade inlet axial Reynolds number | $Re_x$ | $1.1 \times 10^5$ |
| Rotational Reynolds number | $Re_\phi$ | $4.0–9.6 \times 10^6$ |
| Density ratio | $\rho_P/\rho_\infty$ | 1.0–2.0 |

the test matrix and data collection in the turbine are greatly simplified. $SF_6$ has a molecular weight of 146.06 g/mol, which is considerably heavier than air (28.97 g/mol). For this reason, seeding of the $SF_6$ tracer gas, $c_s$, was kept at a minimal concentration of 0.05% (500 ppm) to prevent an increase of the air mixture molecular weight above a 1% change which could influence natural streamlines.

**Turbine Operating Conditions.** The operating conditions for the present study were the same used in previous studies by Monge-Concepción et al. [14] and Siroka et al. [3] and as defined by Berdanier et al. [21] in Table 1. Rim cooling effectiveness data were collected at varying purge and VTE flowrates. Scaled flowrates, $\Phi/\Phi_{ref}$, are presented in this study where $\Phi_p$ is the cooling flowrate of purge, $\Phi_{VTE}$ is the cooling flowrate of VTE flow, and $\Phi_{ref}$ is the reference purge flowrate defined as the flowrate in which the rim seal cavity is fully purged at location B in Fig. 5. For the fully purged condition, the scaled purge flowrate, $\Phi_p/\Phi_{ref}$, equals one.

Propagation of measurement uncertainty related to the test parameters and conditions are presented in Table 2. The uncertainty analysis was performed according to the methodology defined by Figliola and Beasley [22]. To reduce gas analyzer bias uncertainty, both $CO_2$ and $SF_6$ analyzers were zeroed using argon (Ar) gas as a zero-concentration gas. The $CO_2$ analyzer was calibrated daily

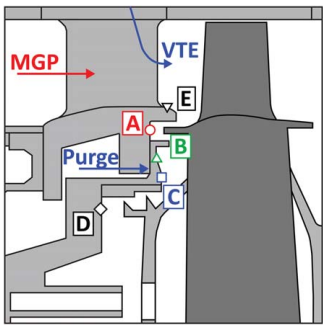


**Fig. 5 Tracer gas sampling locations in the rim seal including front rim seal (location A), front rim cavity (locations B and C), front wheelspace cavity (location D), and vane hub (location E)**

**Table 2 Measurement uncertainties**

| Parameter | Symbol | Value |
|---|---|---|
| Main gas path flow rate | $\dot{m}/\dot{m}_{ref}$ | ±0.004 |
| Shaft rotational speed | $\Omega/\Omega_{ref}$ | ±0.001 |
| Pressures | $P/P_{ref}$ | ±0.001 |
| Temperatures | $T$ | ±0.4 K |
| 1.0 stage pressure ratio | $PR/PR_{ref}$ | ±0.005 |
| Purge flowrate | $\dot{m}_P/\dot{m}_{ref}$ | ±0.018 |
| Purge cooling effectiveness | $\varepsilon_{cc,p}$ | ±0.015 to ±0.025 |
| VTE cooling effectiveness | $\varepsilon_{cc,VTE}$ | ±0.015 to ±0.025 |

using a 1% $CO_2$ concentration supply (gas cylinder) prior to and after testing to confirm no significant change of the analyzer zero and span concentration levels occurred during testing. Similarly, the $SF_6$ analyzer was calibrated daily prior to and after testing using a gas calibration bottle. Local concentration measurement precision of the tracer gas was achieved by averaging data collected over a 30 s time window. Measurement uncertainty ranges for $\varepsilon_{cc,p}$ and $\varepsilon_{cc,VTE}$ shown in Table 2 correspond to the full range of purge and VTE flowrates used in this study.

## Tracer Gas Seeding Configurations

Local gas concentration measurements were collected at four radial locations in the stator–rotor interface, as shown in Fig. 5, including the rim seal (A), rim cavity (B and C), wheelspace cavity (D), and the vane hub (E). A total of four cooling and tracer gas configurations were used to independently evaluate the effect of the purge flow and VTE flow.

Table 3 shows the different tracer gas and cooling flow configurations used in this study; Fig. 6 shows visual representations of each of the cooling flow configurations. The first two sets of studies were the baseline studies, Baseline $CO_2$ and Baseline $SF_6$, to establish a benchmark condition in which the purge flow was varied but included no VTE flow. The difference between baseline $CO_2$ and baseline $SF_6$ studies is the seeding concentration and tracer gas used. In the baseline $CO_2$, the $CO_2$ tracer gas is injected into the purge flow supply line at a molar concentration of 1% (10,000 ppm), while in baseline $SF_6$, the $SF_6$ tracer gas was used as purge flow tracer gas seeded at a molar concentration of 0.05% (500 ppm). The goal of the baseline $SF_6$ configuration study was to evaluate and validate compared to baseline $CO_2$. Previous authors [6,9,23,24] and studies carried out at the START lab [8,15,17,21] have used $CO_2$ as a tracer gas in the purge flow to quantify rim sealing and rim cooling effectiveness. To the authors' knowledge, $SF_6$ as a tracer gas has not been used in the open literature, for which it was imperative to first validate its suitable use.

The third flow configuration is the low VTE configuration similar to the baseline studies only with the constant VTE flow ratio $\Phi_{VTE}/\Phi_{ref} = 0.2$. The fourth flow configuration, referred to as the nominal VTE configuration, is similar to the low VTE configuration. The

**Table 3 Tracer gas configurations**

| Test configuration | MGP background level | Purge flow tracer level | VTE flow tracer level |
|---|---|---|---|
| (1) Baseline $CO_2$ | 0.04% $CO_2$<br>0% $SF_6$ | 1.0% $CO_2$ | No flow |
| (2) Baseline $SF_6$ | 0.04% $CO_2$<br>0% $SF_6$ | 0.05% $SF_6$ | No flow |
| (3) Low VTE | 0.04% $CO_2$<br>0% $SF_6$ | 1.0% $CO_2$ | 500 ppm $SF_6$ |
| (4) Nominal VTE | 0.04% $CO_2$<br>0% $SF_6$ | 1.0% $CO_2$ | 500 ppm $SF_6$ |



Downloaded from http://asmedigitalcollection.asme.org/turbomachinery/article-pdf/145/1/011006/6925311/turbo_145_1_011006.pdf by The Pennsylvania State University user on 03 January 2023

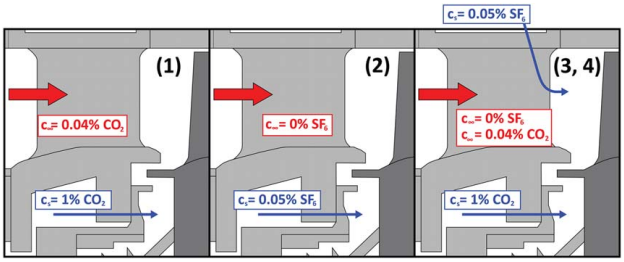


**Fig. 6 $CO_2$ and $SF_6$ seeding configurations: (1) *baseline $CO_2$* configuration, (2) *baseline $SF_6$* configuration, and (3, 4) *low VTE* and *nominal VTE* configurations**

only difference is that the VTE flowrate was introduced at a higher flowrate ratio $\Phi_{VTE}/\Phi_{ref} = 0.4$.

## Benchmarking the Tracer Gases

Although the use of $CO_2$ as a tracer gas has been validated and used successfully in the START test turbine [15,17,21,25], the use of $SF_6$ as a tracer gas is novel and its use had not yet been reported for this application. To successfully measure gas concentrations in the rim seal cavity using $SF_6$, a sampling sensitivity study was necessary to prove that isokinetic sampling could be achieved similar to the $CO_2$ tracer gas.

A benchtop pipe experiment was setup to perform sampling sensitivity studies as shown in Fig. 7, at velocities matching the operational swirl velocities within the test turbine rim seal. The pipe Reynolds number was $Re_D = 1.25 \times 10^5$ and therefore fully turbulent flow was present in the pipe. For the benchmarking, two sets of experiments were performed, beginning with gas concentration samples measured at $x/D = 105$ to determine sampling flowrate sensitivity. In the second experiment, gas concentration was sampled along the length of the pipe to determine concentration development and mixing, and if any differences existed between $CO_2$ and $SF_6$ as tracer gases. Pure $CO_2$ and pure $SF_6$ both non-diluted

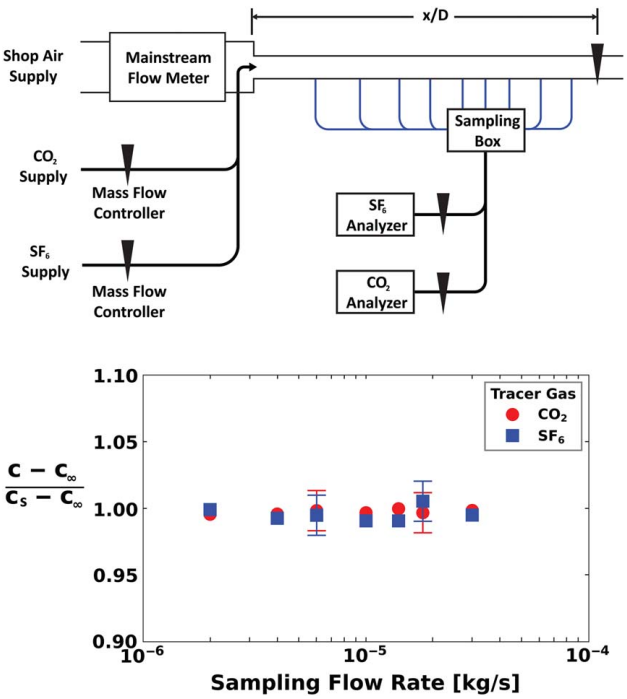


**Fig. 7 Benchtop experiment to validate sampling flowrate sensitivity**

(1,000,000 ppm) were seeded through a pressure tap at the side of the pipe at a non-dimensional distance $x/D = 0$.

For the first benchmarking experiment, gas concentration measurements were acquired at various sampling flowrates at the pipe exit $x/D = 105$ (assumed fully mixed) resulting in a non-dimensional concentration equal to 1, as shown in Fig. 7. The uncertainty bars shown in Fig. 7 correspond to a non-dimensional concentration value $\pm 0.015$. Results show that no significant change was observed over the range of sampling flowrates tested in this experiment. Overall, the results were consistent with those from Clark et al. [17] where even in a compressible flow, as long as the concentration is uniform, the measured concentration was constant with sampling flowrate. For the turbine rig experiments, a sampling flowrate of $10^{-5}$ kg/s was used.

For the second benchmarking experiment, gas concentration measurements were collected along the length of the pipe. It should be noted that the second experiment used a different lower injection flowrate of the tracer gases relative to the first experiment. The lower injection rate was selected for the second experiment in order to better illustrate that the flow mixing process gradually levels out along the pipe length and reaches the expected fully mixed condition at the pipe exit, which was a selected target of 0.75. The results of the second experiment are shown in Fig. 8. Concentration measurements at the entrance of the pipe ($x/D < 20$) are not shown since the tracer gas concentration levels were above the measuring range of the gas analyzers. Figure 8 shows that the non-dimensional concentration was between 0.3 and 0.4 within $20 < x/D < 30$. This reduced concentration was expected since the tracer gases were only injected from one side of the pipe and the flow was not fully mixed in this region. Flow at a length $x/D > 90$ shows that non-dimensional concentration changes less than 5% confirming a fully mixed flow at $x/D = 105$. Comparison of concentration measurements for both $CO_2$ and $SF_6$ in Fig. 8 show nearly the same levels indicating similar flow development and confirming the suitable use of $SF_6$ as a tracer gas.

## Baseline Rim Sealing Effectiveness

Two baseline studies, baseline $CO_2$ and baseline $SF_6$, were conducted to benchmark the turbine operating point when purge flow was present in the stator–rotor cavity interface but VTE flow was not present in the turbine main annulus ($\Phi_{VTE}/\Phi_{ref} = 0$). For these baseline tests, both tracer gases were injected into the purge flow during two separate experiments. Results of the baseline studies are shown in Fig. 9 as a function of the purge mass flowrate ratio ($\Phi_p/\Phi_{ref}$). Since the purge flow is the only source of secondary flow present in the rim seal cavity, the conventional definition of rim sealing effectiveness applies.

Similar to previous studies [14,15], the rim sealing effectiveness increased with increasing purge flowrate. Figure 9 shows the same effectiveness results in both cases of baseline $CO_2$ and baseline $SF_6$ within an uncertainty of $\varepsilon_c = \pm 0.025$. This similarity in rim sealing effectiveness confirms that the use of $SF_6$ as a tracer gas does not change the rim seal flowfield. Despite the differences in the molecular weight and chemical composition, the two tracer gas results were nominally the same.

## Influence of Vane Trailing Edge Flow on Rim Effectiveness

To quantify the VTE flow influence on the rim seal behavior, two VTE flows were included: low VTE and nominal VTE. The low VTE configuration used a constant VTE mass flowrate ratio of $\Phi_{VTE}/\Phi_{ref} = 0.2$ while the nominal VTE configuration used $\Phi_{VTE}/\Phi_{ref} = 0.4$. The tracer gas configurations used for both studies included $CO_2$ with a molar concentration of 1% for the purge flow, and $SF_6$ with a molar concentration of 0.05% for the VTE flow. Rim cooling effectiveness results are presented since the

Downloaded from http://asmedigitalcollection.asme.org/turbomachinery/article-pdf/145/1/011006/6925311/turbo_145_1_011006.pdf by The Pennsylvania State University user on 03 January 2023

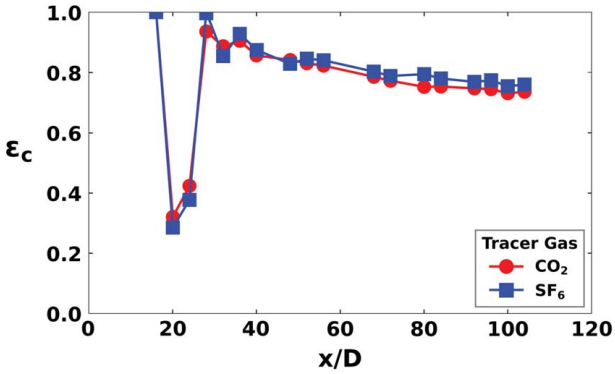


**Fig. 8 Benchtop experiment to validate non-dimensional concentration development along the length of the pipe**

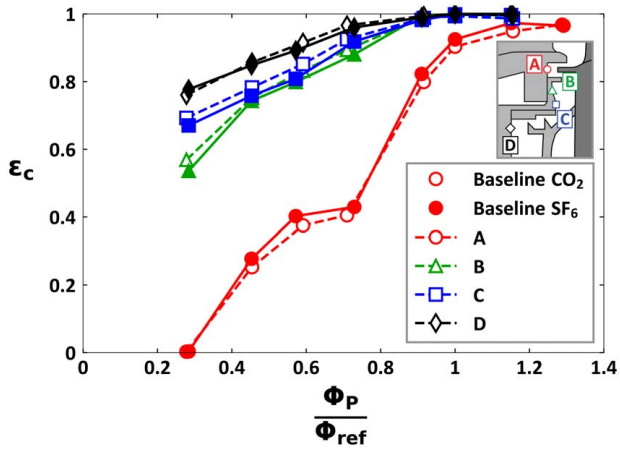


**Fig. 9 Baseline $CO_2$ and baseline $SF_6$ rim sealing effectiveness results at locations A, B, C, and D. Open symbols are the baseline $CO_2$ results and solid symbols are the baseline $SF_6$ results.**

VTE flow originates from the main gas path annulus and mixes with the main annulus inlet flow.

Figure 10 shows the purge flow rim cooling effectiveness ($\varepsilon_{cc,p}$) plotted on the ordinate for the four distinct radial locations in the rim seal cavity corresponding to the locations in Fig. 5. Baseline $CO_2$ results are shown in dashed lines with open symbols, the low VTE results are shown in dotted lines with contrast-colored solid symbols, and the nominal VTE results are shown in solid lines with solid colored symbols.

Observation of the $\varepsilon_{cc,p}$ results in Fig. 10 show that at the inboard locations in the rim seal cavity (locations B, C, and D) the presence of VTE flow does not significantly affect or change the influence of purge flowrate for the two VTE flowrates considered (low VTE and nominal VTE). For location A, the results of $\varepsilon_{cc,p}$ show that VTE flow does affect the cooling effectiveness measurements relative to the baseline results without VTE flow. The data at location A indicate that as the VTE flow increases from $\Phi_{VTE}/\Phi_{ref} = 0$ to 0.4, the effectiveness of purge flow decreases. This will be explained when discussing effectiveness results of the VTE flow, $\varepsilon_{cc,VTE}$.

Given two distinct tracer gases are used, the opportunity to differentiate the direct influences of the purge flow versus the VTE flow can be achieved. Comparison of $\varepsilon_{cc,p}$ results between the baseline studies and the configurations in which VTE flow is present showed that the inboard locations (B, C, and D) were mostly unaffected by the presence of VTE flow. The influence of VTE flow was measured using the $SF_6$ concentration in the rim cavity and wheelspace. Since $SF_6$ was only seeded in the VTE flow, $SF_6$ is a direct measurement of VTE flow in the rim seal and wheelspace cavities. Figure 11 shows the influence of VTE flow presence on rim cooling effectiveness ($\varepsilon_{cc,VTE}$) for various purge flowrates. The data show that the influence of VTE flow presence on rim cooling effectiveness ranges from $0.0 < \varepsilon_{cc,VTE} < 0.15$. Results show that the presence of VTE flow decreases as purge flowrate ratio increases regardless of location in the rim seal cavity and VTE flowrate. This phenomenon was also observed previously by Monge-Concepción et al. [15] and suggested that the behavior is due to the increased pressure within the rim seal cavity, which reduces ingestion of both the hot main annulus flow and VTE flow.

Effectiveness results at the inboard locations (B, C, and D) in Fig. 11 show that the presence of VTE flow is lower than at the rim seal (location A). Location A can be observed to be receiving the most exposure of the VTE flow migrating from the main gas path regardless of VTE flowrate. An increase of VTE flowrate ratio from $\Phi_{VTE}/\Phi_{ref} = 0.2$ to 0.4 was also observed to increase the $\varepsilon_{cc,VTE}$ across all radial locations and all tested purge flow ratios. However, the location mostly affected by the increase of VTE flowrate was location A in which $\varepsilon_{cc,VTE}$ increased from $\varepsilon_{cc,VTE} = 0.07$ to 0.15. These results indicate that higher VTE flowrates can potentially further decrease the fluid temperature in the rim seal cavity. Locations particularly closer to the VTE flow origin have the most potential of benefiting from the lower air temperatures.

Since different tracer gases were used to determine the independent contribution of each cooling flow, a superposition relationship between all cooling flows could be used, as was previously shown valid by Monge-Concepción et al. [15]. This relationship is given in Eq. (1) where rim cooling effectiveness ($\varepsilon_{cc}$) is a combination of the independent contributions of purge flow ($\varepsilon_{cc,p}$) and VTE flow ($\varepsilon_{cc,VTE}$).

$$\varepsilon_{cc} = \varepsilon_{cc,p} + \varepsilon_{cc,VTE} \tag{1}$$

Figure 12 shows rim cooling effectiveness resulting from the superposition of effectiveness results from Figs. 10 and 11. Each of the subplots in Fig. 12 shows results for the baseline $CO_2$, low VTE, and nominal VTE configurations for all sampling locations (similar to Fig. 10). As VTE flow increases, the total rim cooling effectiveness increases, confirming the inherent benefit of VTE flow for cooling. Recalling the results of $\varepsilon_{cc,p}$ from Fig. 10, a decrease of effectiveness was shown at location A for purge flowrates $\Phi_P/\Phi_{ref} > 0.8$. This decrease is due to the presence of VTE flow at location A. As the purge flow increases for a constant VTE flow, a fraction of VTE flow migrates from the annulus into the rim seal cavity.

The use of multiple tracer gases allowed for independent measurements of each cooling flow present in the rim seal and wheelspace cavities. The distribution of ingested cooling flows and hot main annulus flow into the rim seal cavity is of great interest to engine designers. Recall that concentration effectiveness is a mass transfer analogy which relates the purge mass flow ($\dot{m}_p$) to the total egress flow from the rim seal ($\dot{m}_e$). Concentration effectiveness is the ratio of the purge flow in the rim seal to the total egress flow from the rim seal cavity, $\varepsilon_{cc} = \dot{m}_p/\dot{m}_e$.

To determine the distribution of the total rim seal flow, the sum of all individual flows present in the rim seal region can be taken and normalized with respect to the total egress flow as shown in Eq. (2):

$$\frac{\dot{m}_p}{\dot{m}_e} + \frac{\dot{m}'_{VTE}}{\dot{m}_e} + \frac{\dot{m}'_{MGP}}{\dot{m}_e} = 1 \tag{2}$$

where $\dot{m}'_{VTE}$ is the mass fraction of ingested VTE flow into the rim seal and $\dot{m}'_{MGP}$ is the mass fraction of main gas path flow ingested into the rim seal. Equation (3) can be further simplified as

$$w_p + w_{VTE} + w_{MGP} = 1 \tag{3}$$

The term $w_p$ is the mass fraction of purge flow $w_p = \varepsilon_{cc,p}$, while the term $w_{VTE}$ is the mass fraction of ingested VTE flow $w_{VTE} = \varepsilon_{cc,VTE}$.

Figure 13 shows the distribution of each individual flow present in the rim seal (location A). The bar groupings correspond to the baseline, the low VTE, and the nominal VTE configurations. Results show that as purge flow increases, the fraction of the



Downloaded from http://asmedigitalcollection.asme.org/turbomachinery/article-pdf/145/1/011006/6925311/turbo_145_1_011006.pdf by The Pennsylvania State University user on 03 January 2023

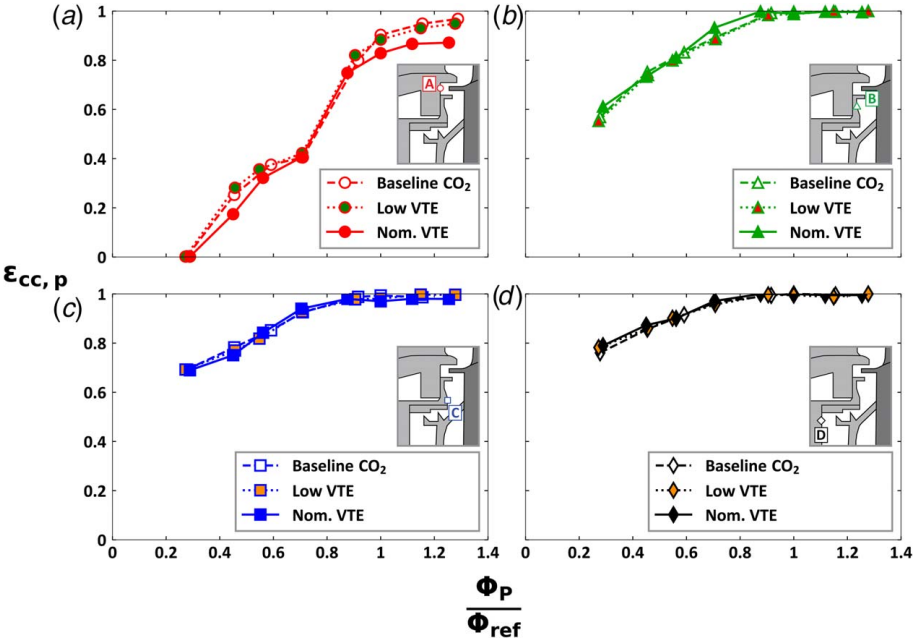


**Fig. 10 Influence of purge flow on rim cooling effectiveness using $CO_2$ as a tracer gas at locations A, B, C, and D (*a*)–(*d*)**

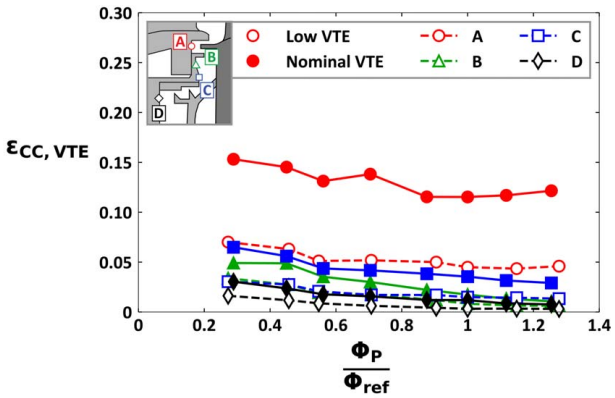


**Fig. 11 Influence of VTE flow on rim cooling effectiveness using $SF_6$ as a tracer gas at locations A, B, C, and D**

purge flow in the rim seal increases, where an increase in purge flow pressurizes the rim seal, reducing main gas path ingestion. Similarly, an increase in purge flow decreases the presence of main gas path ingestion, as shown by the upper stacked bars. The presence of ingested VTE flow in the rim seal is shown to remain mostly constant with respect to all flows present in the rim seal.

Figure 13 also shows that as the purge flowrate on the *x*-axis increases, the relative amount of ingested VTE flow, $\dot{m}'_{VTE}$, also increases with respect to the total ingress flow, $\dot{m}_i$. This phenomenon was previously observed by Scobie et al. [12] in which their study showed re-ingested purge flow into the downstream rim seal cavity increased as the purge flowrate increased. An explanation of why $w_{MGP}$ decreases and $w_{VTE}$ remained constant when purge flow increased is related to the VTE flow at the inner wall of the annulus within the boundary layer (rather than main gas path flow in the case of Scobie et al. without VTE flow). The VTE flow close to the wall does not fully mix with the rest of the annulus flow and, as such, results in a concentration of VTE flow that remains largely invariant as flow exits from the VTE and makes its way into the stator–rotor entrance. A physical explanation of this phenomenon is discussed in the following section.

The results in Fig. 13 also indicate that at purge flowrates of $\Phi_p/\Phi_{ref} > 1$, where the rim seal cavity is fully sealed in the baseline configuration, there is still a presence of both VTE flow and main gas path ingestion for both the low and high VTE configurations. This difference between the baseline results and the cases where VTE flow is present demonstrate that the front rim seal is not fully sealed due to a change in the main annulus boundary condition by the presence of the VTE flow. Although there is still a presence of main gas path ingestion at purge flowrates $\Phi_p/\Phi_{ref} > 1$ for the configurations with VTE flow, the detrimental effect of the main hot gas path flow is reduced by the cooling benefit VTE flow carries into the rim seal.

In a previous study by Siroka et al. [3], they found that a decrease in fluid temperature was observed when a nominal VTE flowrate was present in the rim seal. This finding confirmed that VTE flow ingress has cooling potential to the rim seal. The findings shown in Fig. 13 provide engine and secondary air system designers a better understanding of the flow distribution present in the rim seal at varying purge flowrates. These results show that the presence of VTE flow in the rim seal is important to the flow physics of ingestion, which is currently not included in empirical models. The results and analyses in this study show the benefits of using multiple tracer gases to quantify the different flows involved in hot gas ingestion and rim sealing. This methodology is novel in gas turbine research and can be further utilized in research topics aimed at quantifying distinctly different flows.

## Mass Fraction of Ingested Vane Trailing Edge Flow

As cooling flow exits from the vane trailing edge slots, the VTE flow mixes with the main gas path annulus flow. The benefits of having two tracer gases are that it allows quantifying the fraction of VTE flow relative to the main gas path flow that gets ingested into the rim seal region, and also allows the two cooling flows (purge and VTE flow) to be completely distinguished from each other. This section of the paper discusses the circumferential variation of VTE flow with respect to the total ingress flow. A CFD model was used to qualitatively compare simulation results with experimental results to further explain the flow physics involved in the VTE flow ingestion process.

**Circumferential Variation of Vane Trailing Edge Ingress.** Concentration effectiveness presented previously in this paper



Downloaded from http://asmedigitalcollection.asme.org/turbomachinery/article-pdf/145/1/011006/6925311/turbo_145_1_011006.pdf by The Pennsylvania State University user on 03 January 2023

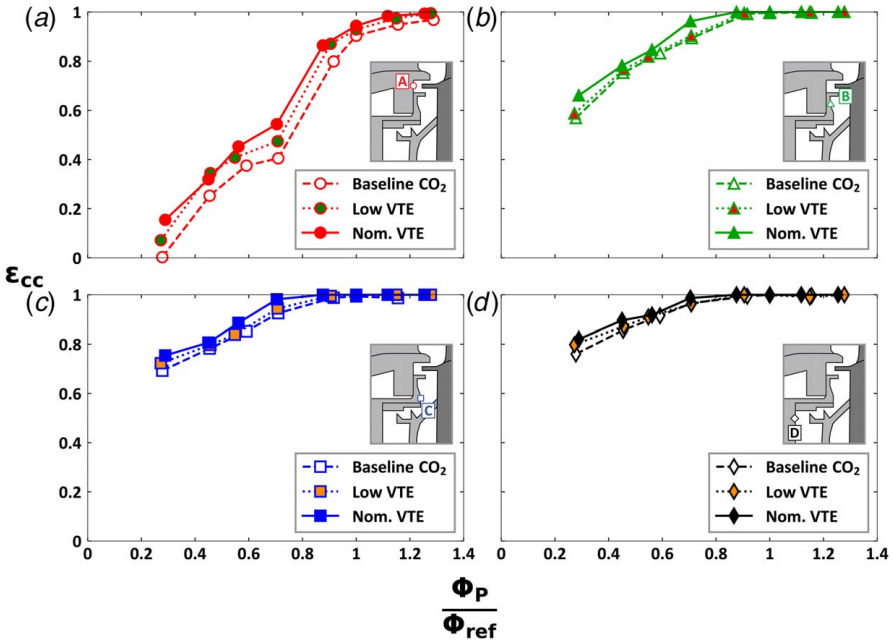


**Fig. 12 Rim cooling effectiveness ($\varepsilon_{cc}$) calculated from independent contributions of each cooling flow using superposition, as proposed in Ref. [15]**

have been circumferentially averaged at each radial location. Although this practice is consistent with previous authors, the circumferential spatial distribution is not known. Previous results by Clark et al. [25] have shown rim sealing effectiveness circumferential variation at various purge flowrates. To date, no studies have presented a variation of circumferential ingestion of VTE flow.

The parameter $\chi$ was defined by Scobie et al. [12] as the mass fraction of egress flow from the upstream portion of the rim seal cavity that is re-ingested into the downstream portion of the rim seal cavity. This mass fraction was normalized with respect to the total ingress flow which was a mixture of re-ingested flow and main gas path flow in the annulus. Similarly, $\chi_{VTE}$ is the mass fraction of ingested VTE flow ($\dot{m}'_{VTE}$) into the rim seal with respect to the total ingestion ($\dot{m}_i$). To quantify $\chi_{VTE}$ in terms of measurable effectiveness values, Eq. (4) is defined:

$$\chi_{VTE} = \frac{\varepsilon_{cc,VTE}}{1 - \varepsilon_{cc,p}} \tag{4}$$

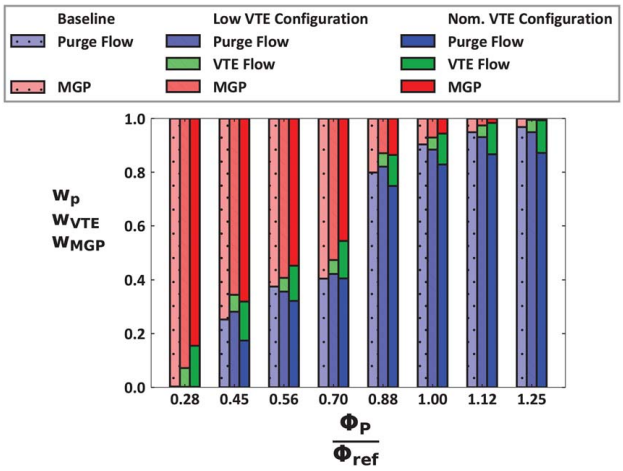


**Fig. 13 Mass fraction distribution of purge flow and main gas path ingested flow in the rim seal (location A) for both the low VTE and nominal VTE configurations**

where $\varepsilon_{cc,VTE}$ is the contribution of VTE flow to rim cooling effectiveness and $\varepsilon_{cc,p}$ is the contribution of purge flow to rim cooling effectiveness. The term $1 - \varepsilon_{cc,p}$ corresponds to the total ingestion flow into the rim seal cavity.

Circumferential variation of VTE ingestion was studied at three pitch locations as shown in Fig. 14. The pitch location 0 s was defined by the intersection between the vane exit metal angle and the downstream vane platform. A full pitch, $s$, was defined as the circumferential distance between two vane trailing edges. The circumferential pitch positions at which experimental data were collected represent 0 s, 0.5 s, and 0.7 s at location A in the front rim seal (refer Fig. 5).

The circumferential variation of ingested VTE flow was quantified in terms of mass fraction ($\chi_{VTE}$) and plotted in Fig. 15 using low and nominal VTE flow. As purge flow increases, $\chi_{VTE}$ also increases across all pitch locations at the front rim seal. The portion of ingested VTE flow ($\dot{m}'_{VTE}$) also increases as purge flow increases, such that the total ingested flow contains less main gas path fluid ($\dot{m}'_{MGP}$). Further observation of results in the nominal VTE configuration shows that $\chi_{VTE}$ decreases as pitchwise location increases away from the discrete trailing edge injection location.

These findings show that the discrete injection of VTE flow from the airfoils also creates non-uniform circumferential variations in the rim seal, which confirms that VTE flow is not fully mixed in the front rim seal. As the cooling flow exits the vane trailing edge slots, the VTE flow is mostly a low-momentum jet in comparison to the main gas path flow. The VTE flow closest to the hub endwall is entrained within the wall boundary layer where it partially mixes with the main gas path flow and is ingested into the rim seal at localized pitch locations.

Overall results in Fig. 15 show that mostly constant values of $\chi_{VTE}$ are reported at purge flowrates $\Phi_p/\Phi_{ref} < 0.6$, which correspond to purge flowrates below the region of inflection in the rim sealing effectiveness curves, as shown at location A in Figs. 9 and 10. The constant fraction of ingested VTE flow in this purge flow regime is a result of slow influential growth of purge flow effectiveness ($\varepsilon_{cc,p}$), as shown in Figs. 9 and 13. At the purge flowrates above the inflection region, $\Phi_p/\Phi_{ref} > 0.6$, $\chi_{VTE}$ increases at a higher rate than at lower purge flows. This rapid increase in $\chi_{VTE}$ is also observed in Fig. 13 for $\Phi_p/\Phi_{ref} > 0.6$ where there is a significant reduction of the ingested hot main annulus flow present in the front rim seal (upper bars in Fig. 13) due to a rapid increase of $\varepsilon_{cc,VTE}$ at location A past the effectiveness inflection region, as shown in Fig. 10(*a*).

Downloaded from http://asmedigitalcollection.asme.org/turbomachinery/article-pdf/145/1/011006/6925311/turbo_145_1_011006.pdf by The Pennsylvania State University user on 03 January 2023

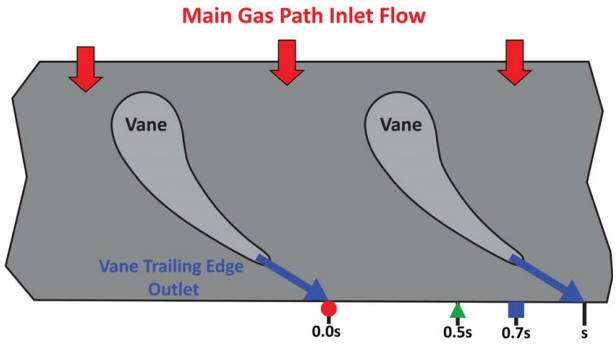


**Fig. 14 Circumferential pitch locations of gas sampling taps in the rim seal at location A**

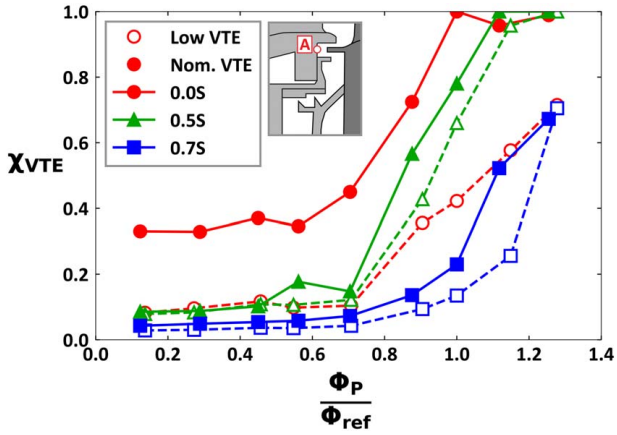


**Fig. 15 Calculated $\chi_{VTE}$ with respect to purge mass flow ratio at three circumferential locations, as indicated in Fig. 14**

Comparison of results in Fig. 15 shows that higher values of $\chi_{VTE}$ are observed in the nominal VTE configuration when compared to the low VTE configuration. These findings are consistent with results shown in Fig. 13 where the lower VTE flowrates contribute to less presence of VTE flow in the front rim seal. A particular result in Fig. 15 that is contrary to the nominal VTE configuration is the pitch 0.0 s and 0.5 s results in the low VTE configuration. Notice that the $\chi_{VTE}$ results at 0.5 s pitch are higher than those observed at 0.0 s for the low VTE configuration. A reduction of VTE flow implies a reduction of the momentum in the VTE flow jet. This reduction of the VTE flow results in a stronger flow turning towards the circumferential direction of the rotating turbine blades as axial momentum of the VTE flow is reduced.

**Computational Fluid Dynamics Model of Vane Trailing Edge Flow Ingestion.** To further understand the effect of VTE flow ingestion, an unsteady Reynolds-averaged Navier–Stokes (URANS) model was interrogated. The CFD model used represents the full turbine stage in the experimental rig and captures the flow interactions of the main gas path flow with rim seal cavity flows. The computational domain is a quarter-wheel circumferential sector of the turbine stage. The turbine stage geometry was meshed using a commercial software [26] and then exported to commercial CFD code [27]. The turbulence model used was a $k$–$\omega$ shear stress transport model. Details of the meshing process, mesh quality, grid independence study, and turbulence model setting are described in further detail by Robak et al. [28].

Figure 16 shows contour plots of the vane inner wall of (a) coefficient of pressure and (b) VTE flow contribution to rim cooling effectiveness. Both plots correspond to a non-dimensional purge flowrate of $\Phi_p/\Phi_{ref} = 0.7$ and a non-dimensional VTE flowrate of $\Phi_{VTE}/\Phi_{ref} = 0.4$. The coefficient of pressure ($C_p$) presented in Fig. 16(*a*) was normalized by purge plenum density ($\rho$) and reference pressure ($P_{ref}$) was taken at location A in Fig. 5. Rim cooling effectiveness results of VTE flow ($\varepsilon_{cc,VTE}$) varies from 0 to 1 where 0 corresponds to no VTE flow present and 1 corresponds to all flow present is from the VTE flow. The line labeled "platform" marks the end wall where the stator wall is located in the rim seal cavity. The platform line marks the entrance to the front rim seal.

An increase in static pressure is shown at the vane trailing edge as shown in Fig. 16(*a*) as flow exits the VTE. Coefficient of pressure contours in Fig. 16(*a*) show a wide region of negative coefficient of pressure along the suction side of the vane. In this region of negative coefficient of pressure, ingress is caused by the entrainment of the VTE flow into the front rim seal as shown by the negative symbol in Fig. 16(*a*). The opposite occurs in the regions of positive coefficient of pressure, where egress occurs. Observation of results in Fig. 16(*b*) shows the VTE flow exiting the vane trailing edge outlet is mostly localized. This jet remains concentrated past the vane platform after which the VTE flow fully mixes with the annulus flow. Figure 16(*b*) strongly suggests that VTE flow in the annulus is mostly localized and does not fully mix at the VTE outlet.

Axial cross-sectional planes were taken from the computational predictions to observe the flow vectors at two distinct pitches. Figure 17 shows contours of the VTE rim cooling effectiveness ($\varepsilon_{cc,VTE}$) in vane hub, front rim seal, and rim seal cavity with flowfield velocity vectors overlaid. The vectors were projected into the axial cut plane and included to visualize flow migration from the turbine annulus into the rim seal. The two vane pitches plotted in Fig. 17 are shown to correspond to (a) 0 s and (b) 0.5 s. Figure 17 shows that VTE flow is mostly entrained in the inner annulus wall which suggests that VTE flow is primarily carried by the inner wall boundary layer. Consistent with previous results, the VTE flow at the edge of the vane hub and vane platform varies with circumferential location. At pitch 0 s (Fig. 17(*a*)), the presence of VTE flow at the inner hub is more significant when compared to results in a pitch of 0.5 s (Fig. 17(*b*)). The results in the inner hub wall suggest that there is variation of VTE flow in the main gas path.

Flow vectors in Fig. 17 were included to visualize flow migration in the rim seal and rim seal cavities. At pitch 0 s, a strong recirculation zone occurs in the blade platform at the entrance of the front rim seal when compared to CFD results at pitch 0.5 s. VTE flow in this recirculation zone mixes with main gas path flow and the concentration of VTE flow decreases. The recirculation zone in the blade platform was previously reported by Gibson et al. [29]. Results for pitch 0 s show the ingestion of VTE flow into the front rim seal. Both pitch locations show that the highest concentration of VTE flow is along the stator wall. This is consistent to predictions of ingress by Owen [2] where ingestion from main gas path, which potentially includes VTE flow, occurs along the stator wall. Furthermore, vectors also confirm egress along the disk wall and flow egresses the rim seal due to flow being pumped out (disk pumping) of the rim seal cavity. The axial cut corresponding to pitch 0 s cuts close to the center of the purge hole at radial location C, as shown in Fig. 17(*a*). As flow exits the purge hole, the flow splits into two recirculation zones. The top zone flow is shown to be pumped out by the disk; for the bottom zone, the flow is shown to be pulled toward the knife-edge seal which leads to the front wheelspace cavity (location D in Fig. 5).

One discrepancy between the experiments and the computational predictions is that the CFD under predicts the magnitude of the VTE flow ingestion into the front rim seal and rim seal cavity. The $\varepsilon_{cc,VTE}$ CFD results in the front rim seal are in a range of $\varepsilon_{cc,VTE} < 0.1$ compared to the experimental results in the front rim seal of $0.11 < \varepsilon_{cc,VTE} < 0.15$ as shown in Fig. 11. Under predicting the VTE ingestion is consistent with previous CFD results reported by Robak et al. [28] in which the URANS model tends to over predict rim sealing effectiveness and under predicts hot gas ingestion into the rim seal. For the cases presented in this paper, where VTE flow is present, VTE flow ingestion in the CFD model is under predicted and $\varepsilon_{cc,VTE}$ in the front rim seal is around 0.04.

Downloaded from http://asmedigitalcollection.asme.org/turbomachinery/article-pdf/145/1/011006/6925311/turbo_145_1_011006.pdf by The Pennsylvania State University user on 03 January 2023

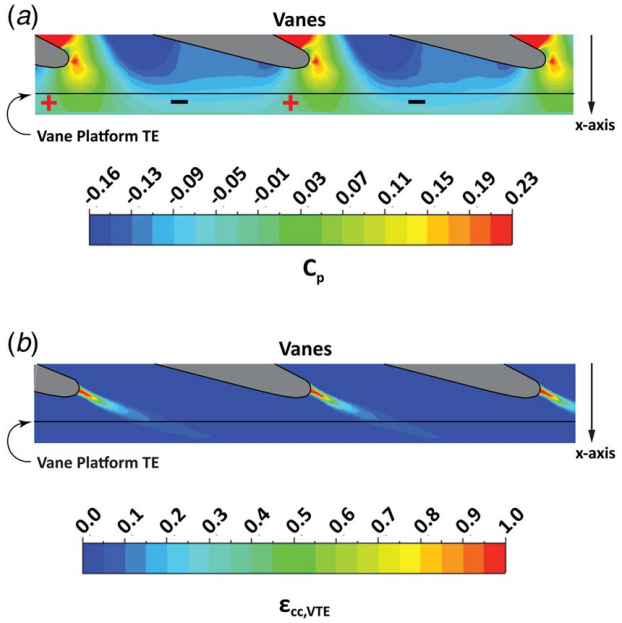


**Fig. 16 Vane inner wall showing vane trailing edge. Contours shown correspond to (*a*) coefficient of pressure and (*b*) VTE flow rim cooling effectiveness**

Furthermore, comparison of results between the two pitches shows that circumferential variation of VTE ingestion is predicted. Results shown in Fig. 17 show that as VTE flow is ingested into the rim seal, it mostly mixes with the rest of the hot gas ingestion. As the flow continues into the rim seal cavity, it is already mostly mixed out which is a challenge for predicting especially in this area of a turbine because of the turbulent energy dissipation model in locations where there is a dramatic change in Mach numbers between annulus flow and rim seal flow [28,30,31].

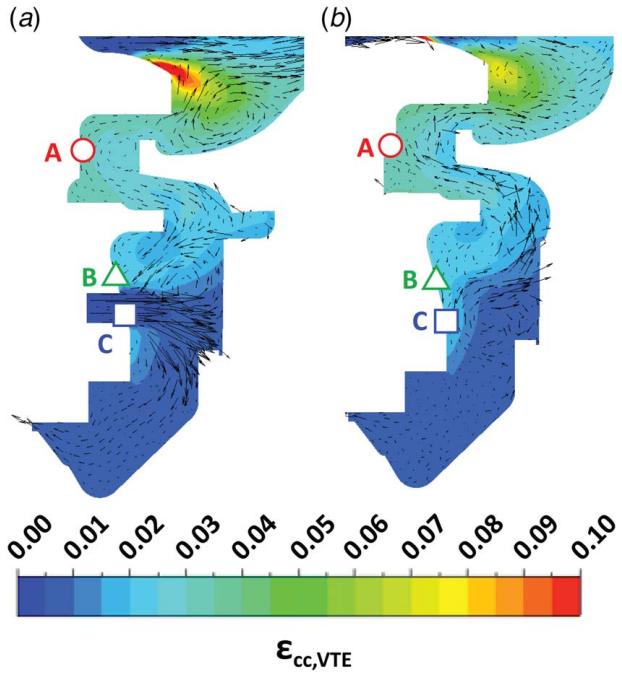


**Fig. 17 CFD simulation results of VTE ingestion into the front rim seal and the rim seal cavity at pitch locations: (*a*) 0 s and (*b*) 0.5 s**

## Conclusions

A comprehensive study was performed to evaluate the effect of VTE flow on rim cooling effectiveness using a one-stage turbine rig operated with engine-realistic geometries at engine-relevant conditions. Rim cooling effectiveness was studied using $CO_2$ and $SF_6$ as tracer gases for the turbine cooling flows including purge flow and VTE flow. The $SF_6$ was benchmarked in a series of experiments outside of the turbine rig to characterize the $SF_6$ gas and validate its use as a flow tracer. The benchtop experiments confirmed the suitable use of $SF_6$ as a tracer gas in which it performed similarly to the conventional $CO_2$ tracer gas. Baseline studies of rim sealing effectiveness were then performed in the turbine using only purge flow seeded with $CO_2$ and $SF_6$ in two separate tests. The baseline test results confirmed that the two different tracer gases yielded the same turbine rim sealing performance. The use of $SF_6$ as a tracer gas offers a new opportunity for reduced uncertainty relative to conventional $CO_2$ concentration measurements.

A method was defined to determine the composition of the flow present in the rim seal for two VTE flow conditions over a range of purge flowrates. Results of this method showed that as purge flowrate increased, the rim cooling effectiveness increased and the mass fraction of ingested VTE flow also increased. This method revealed a full profile of the different cooling flows and hot main gas path flow in the rim seal cavity for the first time in open literature. Results showed that at the highest purge flowrates, which were considered to be fully sealed rim cavity conditions in the baseline configurations, ingestion of main gas path flow and VTE flow still occurs in the front rim seal. The fraction of ingested VTE flow can provide beneficial cooling to the front rim seal and rim seal cavities.

A CFD model was used to study the flow physics associated with the VTE ingestion process and validate experimental results. Computational results in the main annulus at the inner wall show that the VTE flow is mostly constrained to jets spanning from the VTE outlets. Concentration of VTE flow in the turbine main annulus was shown to vary circumferentially and was validated by experimental inner vane wall results in the turbine rig. The model was able to validate that VTE flow migration occurs from the main gas path into the front rim seal but the magnitude of the VTE flow ingestion was under predicted by the model. Similarly, the circumferential nonuniformities of the VTE flow ingestion at the front rim seal location were not captured by the CFD model. Instead, the CFD predicted a more mixed out combination of the ingested VTE flow and hot main gas path flow as the combined flow migrated into the rim seal.

The migration of VTE flow from the main gas path and into the rim seal shows that there can be a positive cooling potential to the turbine under platform region. The VTE flow migration is currently not included in hot gas ingestion models for which the current study points to the need for further studies. Accurate hot gas ingestion models are needed to account for all turbine cooling effects to further improve turbine efficiencies and more accurately account for component life. A reduction in the use of the secondary airflow system, which includes the purge and VTE flows, can potentially lead to improvements in engine efficiencies and further increase propulsion work output.

## Acknowledgment

The authors would like to thank Pratt & Whitney and the U.S. Department of Energy National Energy Technology Laboratory for sponsoring research presented in this paper. This paper is based upon work supported by the Department of Energy under Award Number DE-FE0025011.

## Disclaimer

This report was prepared as an account of work sponsored by an agency of the United States Government. Neither the United States Government nor any agency thereof, nor any of their employees,

Downloaded from http://asmedigitalcollection.asme.org/turbomachinery/article-pdf/145/1/011006/6925311/turbo_145_1_011006.pdf by The Pennsylvania State University user on 03 January 2023

makes any warranty, express or implied, or assumes any legal liability or responsibility for the accuracy, completeness, or usefulness of any information, apparatus, product, or process disclosed, or represents that its use would not infringe privately owned rights. Reference herein to any specific commercial product, process, or service by trade name, trademark, manufacturer, or otherwise does not necessarily constitute or imply its endorsement, recommendation, or favoring by the United States Government or any agency thereof. The views and opinions of authors expressed herein do not necessarily state or reflect those of the United States Government or any agency thereof.

## Conflict of Interest

There are no conflicts of interest.

## Data Availability Statement

The datasets generated and supporting the findings of this article are obtainable from the corresponding author upon reasonable request.

## Nomenclature

$b$ = hub radius
$c$ = gas concentration
$\dot{m}$ = mass flowrate
$\dot{m}'$ = mass flowrate of ingested flow
$r$ = radius
$w$ = mass fraction of flow present with respect to total egress flow, $\dot{m}/\dot{m}_e$
$C$ = chord length
$P$ = pressure
$S$ = vane pitch length
$V$ = main gas path velocity
$s_c$ = seal clearance
$C_p$ = coefficient of pressure, $(P - P_{\text{mean}})/(0.5\rho\Omega^2 b^2)$
PR = pressure ratio, $P_{\text{in}}/P_{\text{out}}$
$\text{Re}_x$ = axial Reynolds number, $V_x C_x/\nu$
$\text{Re}_\phi$ = rotational Reynolds number, $\Omega b^2/\nu$
$\beta$ = swirl ratio, $V_\phi/\Omega r$
$\varepsilon_c$ = sealing effectiveness, $(c - c_\infty)/(c_s - c_\infty)$
$\varepsilon_{cc}$ = cooling effectiveness, $(c - c_{\infty,\text{in}})/(c_s - c_{\infty,\text{in}})$
$\varepsilon_{cc,p}$ = purge contribution, $(c - c_{\infty,\text{in}})/(c_s - c_{\infty,\text{in}})|_p$
$\varepsilon_{cc,\text{VTE}}$ = VTE contribution, $(c - c_{\infty,\text{in}})/(c_s - c_{\infty,\text{in}})|_{\text{VTE}}$
$\nu$ = kinematic viscosity
$\rho$ = density
$\Phi$ = cooling flowrate, $\dot{m}/(2\pi s_c \rho \Omega b^2)$
$\Phi_{\text{min}}$ = minimum flow parameter to seal a given location
$\Phi_{\text{ref}}$ = reference flowrate, $\Phi_{\text{min}}$ for location B in the *baseline* configuration
$\Omega$ = angular velocity

### Subscripts, Accents, and Abbreviations

in = inlet conditions
out = outlet conditions
$p$ = purge
ref = generic reference conditions
$x$ = axial direction
$\phi$ = tangential direction
$\infty$ = background level

## References


[1] Owen, J. M., 2011, "Prediction of Ingestion Through Turbine Rim Seals—Part I: Rotationally Induced Ingress," ASME J. Turbomach., **133**(3), p. 031005.
[2] Owen, J. M., 2011, "Prediction of Ingestion Through Turbine Rim Seals—Part II: Externally Induced and Combined Ingress," ASME J. Turbomach., **133**(3), p. 031006.
[3] Siroka, S., Monge-Concepción, I., Berdanier, R. A., Barringer, M. D., and Thole, K. A., 2021, "Correlating Cavity Sealing Effectiveness to Time-Resolved Rim Seal Events in the Presence of Vane Trailing Edge Flow," GT2021-59285.
[4] Scobie, J. A., Sangan, C. M., Michael Owen, J., and Lock, G. D., 2016, "Review of Ingress in Gas Turbines," ASME J. Eng. Gas Turbines Power, **138**(12), p. 120801.
[5] Johnson, B. V., Mack, G. J., Paolillo, R. E., and Daniels, W. A., 1994, "Turbine Rim Seal Gas Path Flow Ingestion Mechanisms," Joint Propulsion Conference and Exhibit, 94-2703.
[6] Sangan, C. M., Pountney, O. J., Zhou, K., Wilson, M., Owen, J. M., and Lock, G. D., 2013, "Experimental Measurements of Ingestion Through Turbine Rim Seals—Part I: Externally Induced Ingress," ASME J. Turbomach., 135(2), p. 021012.
[7] Sangan, C. M., Pountney, O. J., Zhou, K., Owen, J. M., Wilson, M., and Lock, G. D., 2013, "Experimental Measurements of Ingestion Through Turbine Rim Seals—Part II: Rotationally Induced Ingress," ASME J. Turbomach., **135**(2), p. 021013.
[8] Clark, K. P., Johnson, D., Thole, K. A., Robak, C., Barringer, M. D., and Grover, E., 2018, "Effects of Purge Flow Configuration on Sealing Effectiveness in a Rotor–Stator Cavity," ASME J. Eng. Gas Turbines Power, **140**(11), p. 112502.
[9] Gentilhomme, O., Hills, N. J., Turner, A. B., and Chew, J. W., 2003, "Measurement and Analysis of Ingestion Through a Turbine Rim Seal," ASME J. Turbomach., **125**(3), pp. 505–512.
[10] Scobie, J. A., Sangan, C. M., Owen, J. M., Wilson, M., and Lock, G. D., 2014, "Experimental Measurements of Hot Gas Ingestion Through Turbine Rim Seals at Off-Design Conditions," Proc. Inst. Mech. Eng. Part A J. Power Energy, **228**(5), pp. 491–507.
[11] Patinios, M., Ong, I. L., Scobie, J. A., Lock, G. D., and Sangan, C. M., 2018, "Influence of Leakage Flows on Hot Gas Ingress," GT2018-75071.
[12] Scobie, J. A., Hualca, F. P. T., Patinios, M., Sangan, C. M., Owen, J. M., and Lock, G. D., 2018, "Re-Ingestion of Upstream Egress in a 1.5-Stage Gas Turbine Rig," ASME J. Eng. Gas Turbines Power, **140**(7), p. 072507.
[13] Hualca, F. P. T., Horwood, J. T. M., Sangan, C. M., Lock, G. D., and Scobie, J. A., 2020, "The Effect of Vanes and Blades on Ingress in Gas Turbines," ASME J. Eng. Gas Turbines Power, **142**(2), p. 021020.
[14] Monge-Concepción, I., Siroka, S., Berdanier, R. A., Barringer, M. D., Thole, K. A., and Robak, C., 2021, "Unsteady Turbine Rim Sealing and Vane Trailing Edge Flow Effects," GT2021-59273.
[15] Monge-Concepción, I., Berdanier, R. A., Barringer, M. D., Thole, K. A., and Robak, C., 2020, "Evaluating the Effect of Vane Trailing Edge Flow on Turbine Rim Sealing," ASME J. Turbomach., **142**(8), p. 081001.
[16] Barringer, M. D., Coward, A., Clark, K. P., Thole, K. A., Schmitz, J., Wagner, J., Alvin, M. A., Burke, P., and Dennis, R., 2014, "The Design of a Steady Aero Thermal Research Turbine (START) for Studying Secondary Flow Leakages and Airfoil Heat Transfer," GT2014-25570.
[17] Clark, K. P., Barringer, M. D., Thole, K. A., Clum, C., Hiester, P., Memory, C., and Robak, C., 2016, "Using a Tracer Gas to Quantify Sealing Effectiveness for Engine Realistic Rim Seals," ASME Turbo Expo 2016, GT2016-58095.
[18] Riffat, S. B., 1992, *Balancing Airflow in HVAC Systems Using Tracer-Gas Techniques*, Department of Architecture and Planning, School of Architecture, University of Nottingham, www.aivc.org/sites/default/files/airbase_5690.pdf
[19] Bassett, M. R., Shaw, C.-Y., and Evans, R. G., 1981, "An Appraisal of the Sulphur Hexafluoride Decay Technique for Measuring Air Infiltration Rates in Buildings," ASHRAE Trans., **97**(2), p. 2657.
[20] Simmonds, P. G., Rigby, M., Manning, A., Park, J., Stanley, S., McCulloch, K. M., Henne, A., et al., 2020, "The Increasing Atmospheric Burden of the Greenhouse Gas Sulfur Hexafluoride (SF6)," Atmos. Chem. Phys., **20**(12), pp. 7271–7290.
[21] Berdanier, R. A., Thole, K. A., Knisely, B. F., Barringer, M. D., Grover, E. A., and Monge-Concepción, I., 2019, "Scaling Sealing Effectiveness in a Stator–Rotor Cavity for Differing Blade Spans," ASME J. Turbomach., **141**(5), p. 051007.
[22] Figliola, R. S., and Beasley, D. E., 2014, *Theory and Design for Mechanical Measurements*, John Wiley & Sons, Inc., Hoboken, NJ.
[23] Savov, S. S., Atkins, N. R., and Uchida, S., 2017, "A Comparison of Single and Double Lip Rim Seal Geometry," ASME J. Eng. Gas Turbines Power, **139**(11), p. 112601.
[24] Savov, S. S., and Atkins, N. R., 2017, "A Rim Seal Ingress Model Based on Turbulent Transport," GT2017-63531.
[25] Clark, K. P., Barringer, M. D., Johnson, D., Thole, K. A., Grover, E. A., and Robak, C., 2017, "Effects of Purge Flow Configuration on Sealing Effectiveness in a Rotor–Stator Cavity," GT2017-63910.
[26] Siemens PLM Software, 2017, STAR-CCM+ 11.06, Siemens PLM Software, Plano, TX.
[27] ANSYS, 2017, *ANSYS Fluent 18.2*, ANSYS, Canonsburg, PA.
[28] Robak, C., Faghri, A., and Thole, K. A., 2019, "Analysis of Gas Turbine Rim Cavity Ingestion With Axial Purge Flow Injection," GT2019-91807.
[29] Gibson, J., Thole, K. A., Christophel, J., Memory, C., and Thomas, P., 2016, "Pressure Distortion Effects on Rim Seal Performance in a Linear Cascade," GT2016-58098.
[30] Denton, J. D., 2010, "Some Limitations of Turbomachinery CFD," Turbo Expo 2010, GT2010-22540.
[31] O'Mahoney, T. S. D., Hills, N. J., Chew, J. W., and Scanlon, T., 2011, "Large-Eddy Simulation of Rim Seal Ingestion," Proc. Inst. Mech. Eng. Part C J. Mech. Eng. Sci., **225**(12), pp. 2881–2891.


Downloaded from http://asmedigitalcollection.asme.org/turbomachinery/article-pdf/145/1/011006/6925311/turbo_145_1_011006.pdf by The Pennsylvania State University user on 03 January 2023